ISSN 1063-7842, Technical Physics, 2016, Vol. 61, No. 10, pp. 1480–1488. © Pleiades Publishing, Ltd., 2016.
Original Russian Text © V.I. Kornilov, A.V. Boiko, 2016, published in Zhurnal Tekhnicheskoi Fiziki, 2016, Vol. 86, No. 10, pp. 38–46.

GASES AND LIQUIDS

Experimental Modeling of Air Blowing into a Turbulent Boundary Layer Using an External Pressure Flow

V. I. Kornilov* and A. V. Boiko

Khristianovich Institute of Theoretical and Applied Mechanics, Siberian Branch, Russian Academy of Sciences, Institutskaya ul. 4/1, Novosibirsk, 630090 Russia

**e-mail: kornilov@itam.nsc.ru*

Received November 23, 2015; in final form, March 10, 2016

Abstract—We have experimentally investigated the characteristics of an incompressible turbulent boundary layer on a plane plate upon the passive blowing of air through a fine-perforated surface and flushing it by supplying an external pressure flow through a wind tunnel using an intake device equipped with an attachment for draining the boundary layer on the inactive side of the plate. A stable decrease in the local values of the surface coefficient of friction, which reaches 80% at the end of the perforated region, has been detected over the length of the plate. The possibility of controlling surface friction by changing the velocity of the external flow and selecting the meshes and filters at the inlet to the flow passage has been demonstrated.

DOI: 10.1134/S1063784216100170

INTRODUCTION

Further advances in the high-speed air transport, as well as overland transport facilities, are hardly possible without developing new economic method for controlling near-wall flows [1, 2]. The experience in controlling laminar flows [3] is a solid starting foundation for developing efficient methods on action on the turbulent boundary layer. However, certain peculiarities of these flows must be taken into account. As a matter of fact, despite its apparent simplicity, a laminar flow for high Reynolds numbers is a complicated object for analysis. In particular, thin laminar boundary layers are extremely sensitive to the surface defects past which they flow [4]. These defects may be due to inevitable manufacturing tolerance in the structure of an aircraft, the joints and mating of various aerodynamic elements, and contamination from insects or defects that appear as a result of collisions of the leading edge of the wing, as well as the forebody of the fuselage and motorized nacelles with sand particles and fine garbage. Control over this flow past a transport aircraft is obviously a complicated problem. In addition, a boundary layer that streamlines many elements of an aircraft, such as fuselage of a rocket airframe, is in a turbulent state in a wide range of Reynolds numbers. For this reason, the application of artificial methods for controlling turbulent flows (in particular, by passive blowing of a gas [5–10] through a hi-tech fine-perforated surface) appears to be a promising way to reduce the frictional resistance and the total aerodynamic drag, which increases the aerodynamic efficiency of an aircraft. As a result, this will increase the flight range and payload and reduce fuel consumption, as well as direct maintenance charges of the aircraft. Another practical problem in which blowing a liquid through a porous wall is used is also worth noting. We are speaking of the thermal protection of surfaces subjected to the action of high-enthalpy flows (gas turbine blades, combustion chamber walls, and other elements of a rocket engine; see, e.g., [11, 12]).

Our earlier studies [13] were devoted to analyzing the efficiency of passive blowing of air through a hydraulically smooth fine-perforated wall by supplying an external pressure flow in a wind tunnel through the inlet system located directly on the inactive surface of the model. This work is aimed at analyzing the possibility of increasing the efficiency of the passive blowing of air through a modified inlet device located in the external flow and separated from the wall by a system for discharging the boundary layer.

1. EXPERIMENTAL TECHNIQUE, METHOD, AND CONDITIONS

The experiments were carried out in a T-324 subsonic low-turbulence wind tunnel with the working part size $1 \times 1 \times 4$ m at the Khristianovich Institute of Theoretical and Applied Mechanics, Siberian Branch, Russian Academy of Sciences, and covered the range of unperturbed flow velocities U_∞ from 9 to 23 m/s, which corresponds to Reynolds numbers per meter $\mathrm{Re}_1 = (0.60–1.53) \times 10^6\ \mathrm{m}^{-1}$.

Measurements were taken on a model of a plane D16T duralumin plate with the size 2204.5 × 993.0 mm

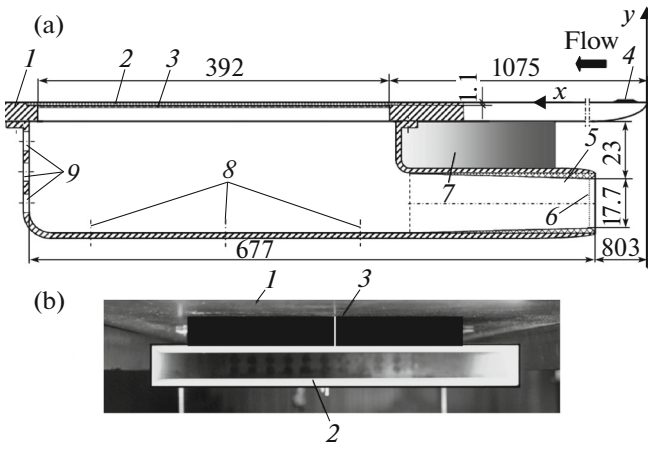

Fig. 1. (a) Diagram of the model (not to scale): (*1*) plane plate; (*2*) fine-perforated sample; (*3*) fine-mesh filter; (*4*) boundary layer turbulizer; (*5*) inlet device; (*6*) mesh + filter; (*7*) boundary layer discharge system; (*8*) pressure gauges; (*9*) adjustable discharge holes; (b) photograph of the inlet device (downstream view): (*1*) inactive side of the plate; (*2*) elliptic edging; (*3*) boundary layer discharge system. (Discharge holes can be seen on the rear wall of the flow channel.)

in the plane and 6 mm in thickness (Fig. 1a). The front and rear sides of plate *1* from the inactive side had the semi-elliptical shape with a semiaxes ratio of 1 : 12. Several static pressure detectors with diameter of 0.4 mm were arranged on the symmetry axis of the plate.

The shape of plate *1* envisaged the possibility of installing a changeable planar fine-perforated sample *2* of thickness $t = 1.1$ mm and a large in-plane size (420 × 250 mm) flush with its main surface, which made it possible to monitor local properties of the flow (average velocity, friction, and velocity pulsations) over a considerable length x. The permeability parameters of the perforated sample, which were chosen using the data from [14], were as follows: the porosity (total relative area of holes) was 17.1%, average diameter $d = 0.17$ mm of holes arranged in the staggered order was, and the ratio $t/d = 6.47$.

In the course of experiment, the incoming pressure air flow entered the rectangular inlet device of size 236.5 × 25.5 mm (Fig. 1b) with rounded (over the entire length of the flow passage) angles, which was arranged directly under the perforated sample. The boundary layer developed on the inactive surface of the model was discharged using attachment *3* of height 18 mm and with the contour of lateral faces of the Vitoshinskii profile. Air from inlet device *5* (see Fig. 1a) was supplied to the boundary layer via an intermediate small-cell double-layer filter SEFAR PET 1500 150/380-34Y *3* and perforated wall *2*.

The choice of the inlet device geometry was based on the following two requirements: the attainment of the flow without separation past the inlet device and obtaining an elevated pressure in the device flow channel. For this purpose, the outsides and the edges of the entrance were profiled in order to obtain minimal aerodynamic drag. In addition, to create these conditions, the rear wall of the channel had controllable delivery orifices *9* with a total area in the open state that constituted 57.8% of the midsection area of the inlet device channel. Pressure heads *8* of diameter 0.4 mm arranged at identical distances from each other served to measure the pressure in the flow channel of the inlet device.

The boundary layer on the working side of the plate was artificially turbulized by placing a 30-mm-long strip *4* of coarse-grain calibrated sand with grain size $h = 0.8$ mm in the region of the maximal variation of pressure (near the leading edge).

Data acquisition and processing in the course of the experiment was carried out directly and analyzed on-line using the software developed based on the MATLAB package. The technique of measuring instantaneous velocity u at the point of the shear flow field under investigation was based on the heat-loss anemometer 55M0 manufactured at DANTEC and was described in detail in [7]. It should only be noted that, as a sensing device, we used a miniature sensor known as a boundary layer probe with a sensitive element in the form of a tungsten filament of diameter 5 μm and length 1.2 mm, which operated at a constant temperature in the overheating regime.

The method of determining the local coefficient of surface friction C_f as the basic parameter in a noncanonical turbulent flow, which in particular can be formed when air is blown into the boundary layer, was substantiated in [15]. It can only be observed that this method makes it possible to take into account the cooling effect of the wall on the reading of the heat-loss anemometer and to correctly describe the velocity distribution in the boundary layer; as a consequence, it yields a value of C_f not only on the logarithmic part of the velocity profile (if it exists), but also (which is especially important) in the region of the laminar sublayer of the turbulent boundary layer used for this purpose.

The random error of measuring the most characteristic quantities can be judged from the results of measuring the local coefficient of surface friction C_f in the investigated range of flow velocities obtained in the absence of the flow using two methods (see table), i.e., from the velocity distribution in the logarithmic region of the boundary layer (law of the wall) and using the original technique extended by the authors to the region of the viscous sublayer. It can be seen that the maximal difference in the values of C_f obtained using these methods is less than 1.0%.

Results of measurement of the local surface coefficient of friction using two different methods (in the absence of the flow)

U_∞, m/s	$\mathrm{Re}_x^\circ \times 10^{-6}$	δ**, mm	$C_f^\circ \times 10^3$		ΔC_f, %
			logarithmic region	laminar sublayer	
9	0.936	3.195	3.399	3.393	0.18
11	1.104	3.145	3.288	3.287	0.03
13	1.305	3.068	3.211	3.210	0.03
15	1.506	3.007	3.135	3.129	0.19
17	1.707	2.934	3.081	3.066	0.49
19	1.908	2.875	3.038	3.024	0.46
21	2.108	2.824	2.980	2.969	0.37
23	2.309	2.777	2.949	2.943	0.20
9	1.037	3.628	3.281	3.262	0.58
11	1.267	3.543	3.175	3.167	0.25
13	1.498	3.438	3.089	3.086	0.10
15	1.728	3.373	3.012	3.001	0.37
17	1.958	3.283	2.963	2.951	0.41
19	2.189	3.224	2.908	2.911	0.10
21	2.419	3.170	2.864	2.845	0.67
23	2.650	3.109	2.838	2.837	0.04

2. RESULTS OF INVESTIGATIONS

2.1. Characteristics of the Flow in the Absence of Air Flow through the Inlet Device (Initial Boundary Layer)

The form of variations in the static pressure on the working surface in the regions of the flow upstream and downstream of the perforated sample indicates that the segment of almost zero-gradient flow are observed in these regions (except in the vicinity of the leading and trailing edges of the plate), in which the static pressure can be considered to be constant to within the experimental error.

The local and integrated parameters of the flow measured directly in the boundary layer show that the shear flow parameters on the perforated surface completely correspond to physical concepts of the properties of the turbulent boundary layer formed on the smooth impenetrable flat plate streamlined by a zero-gradient flow. As an example, Fig. 2 shows the dependence that characterizes the variations in local coefficient of surface friction C_f on number Re**, where Re** is the Reynolds number calculated from the momentum loss thickness δ** of the boundary layer. The results of numerical calculations performed by the authors using the Cebeci technique [16] for a smooth planar plate under the assumption of zero-gradient flow are also given in the figure for comparison. On the whole, satisfactory agreement is observed between the experimental values of C_f obtained by two methods, as well as with the results of numerical calculations. A certain discrepancy between the results is observed on the initial interval of Re** values. However, the maximal deviation of the experimental value of C_f from calculated values (including those obtained on the permeable surface itself) does not exceed 3–4%. This result is a direct confirmation of the important fact that the flow past the fine-perforated wall in the absence of the flow through the inlet device is almost equivalent to the flow past the hydraulically smooth analog.

The behavior of local characteristics of the flow in the inner region of the turbulent boundary layer can be explained by analyzing the mean velocity profiles

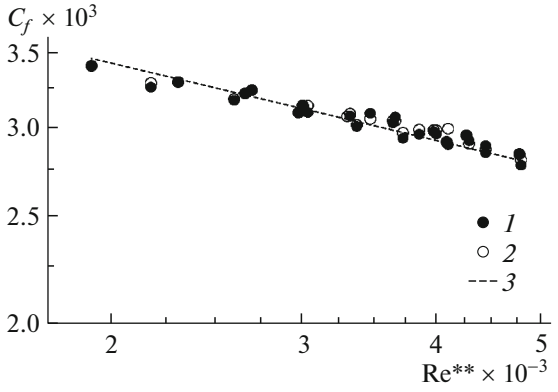

Fig. 2. Dependence of the surface coefficient of friction on the Reynolds number (initial boundary layer, without blowing): (*1*) from the logarithmic region of boundary layer; (*2*) using our technique; (*3*) calculated using by the Cebeci technique.

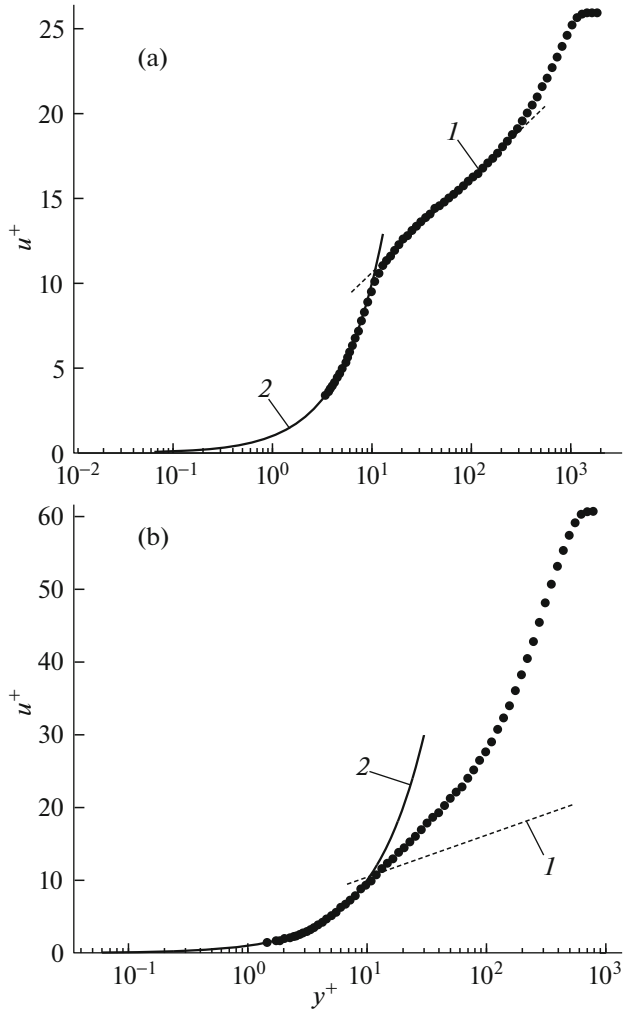

Fig. 3. Average velocity profiles in the boundary layer in the variables of the law of the wall in cross section $x = 1432$ mm: (a) initial boundary layer, without blowing; (b) with blowing, $C_b = 3.95 \times 10^{-3}$; $u^+ = 5.62y^+ + 5.0$ (*1*) and $u^+ = y^+$ (*2*).

measured over the length of the model; an example of such profiles is shown in Fig. 3a in the coordinates of the law of the wall $u^+ = f(y^+)$:

$$u^+ = u/v_*, \quad y^+ = yv_*'/v$$

for cross section x closely spaced from the middle of the perforated sample. It can be seen that the velocity distribution in the logarithmic region of the boundary layer in this case can be satisfactorily described by the classical velocity profile $u^+ = A\log y^+ + B$ with coefficients $A = 5.62$ and $B = 5.0$ [17]. It should also be noted that the experimental distribution of the velocity in the laminar sublayer can be correctly approximated by a linear velocity distribution law $u^+ = y^+$, which makes it possible to determine C_f correctly in the case of blowing into the boundary layer.

The turbulent velocity pulsation profiles in the boundary layer in the variables of the law of the wall $u'/v_* = f(y^+)$ and the Clauser equilibrium parameter $G = [(H - 1)/H](2/C_f)^{0.5}$, where $H = \delta^*/\delta^{**}$ is the form parameter of the boundary layer (see Fig. 10 below) also confirm that, in this case, the characteristics of the shear flow over the perforated wall do not contradict the physical concepts on the properties of a turbulent boundary layer formed on the smooth planar plate in the conditions of the zero-gradient flow.

2.2. Flow Characteristics with an Air Flow through the Inlet Device

In our previous experiments [13], we detected the nonstationary nature of the flow in the channel of the inlet device, which is associated with the formation of the transient regime of flow on the inactive side of the plate. In connection with this, the experiments in this study were carried out under the conditions when the inlet device was brought into the outer flow, but in this case the boundary layer itself was also artificially turbulized. However, this approach was only partially justified. For this reason, we used in addition various combinations of the wire mesh and a fine-meshed filter with a variable permeability, which were installed in the midsection of the inlet device. In this case, the results of measurements of pressure at the lower wall of the flow channel indicate the uniform distribution of pressure over its entire length almost for all regimes of air supply. At the same time, the flow channel for a low penetrability of the mesh + filter combination, e.g., for a high density of the filter, is unable to transmit the air mass flow completely for a preset velocity of the external flow. Indeed, it is well known that the following two main scheme of the flow distorting its normal regime at the inlet can be realized in the flow past the front part of the subsonic air intake:

(i) with the acceleration of the liquid, when the velocities at the inlet are lower than the rated values or if the mass flow rate exceeds the rated value;

(ii) with the deceleration of the liquid, when the inlet velocities exceed the rated values, and the device cannot transmit the entire mass flow due to its structural features.

Experiments show that, for certain mesh + filter combinations at the inlet into the device, the second regime of the flow is realized. This situation was analyzed by visualizing the flow using the method of an oil film that consists of a mixture of titanium dioxide, silicon oil, kerosene, and oleic acid in the volume ratio selected taking into account the low velocity observed in this case. It can be seen (Fig. 4) that the flow lines at the inlet are noticeably bent, and the flow past the lower side of the inlet device is deflected, which indicates that this device cannot transmit the entire mass of air. It suggests that this device cannot ensure minimal losses and the uniform velocity field in the flow part of the channel in these conditions. With increasing penetrability of the mesh + filter combination

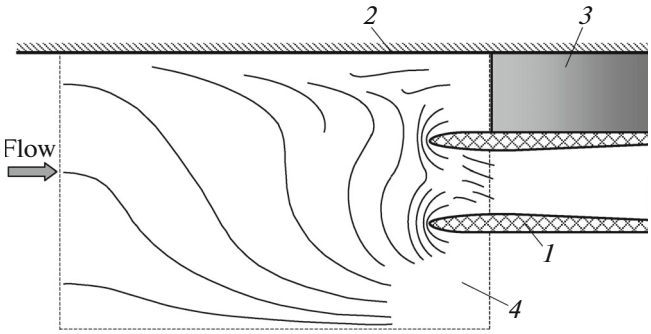

Fig. 4. Pattern of limiting flow lines in the symmetry plane of the inlet device: (*1*) elliptic edging; (*2*) inactive side of the plate; (*3*) boundary layer discharge system; (*4*) visualization plane, $U_\infty = 21$ m/s.

(e.g., upon a decrease in the density of the filter), the curvature of the flow lines decreases, indicating the formation of a more uniform flow at the inlet and an increase in the air flow rate in the flow channel.

Let us now consider some local and integrated characteristics of the shear flow on the perforated surface itself. In this case, the mean velocity profile in the boundary layer in the presence of an air flow through the inlet device is basically the same as for the forced air supply through the pressure chamber [7, 18]. In particular, the velocity distribution in the internal (logarithmic) region of the boundary layer exhibits a clearly manifested deviation of experimental dependence $u^+ = f(y^+)$ from the classical law of the wall (see Fig. 3b). Since variables u^+ and y^+ of the law of the wall are scaled by dynamic velocity $v_* = \sqrt{\tau_w/\rho}$, where τ_w is the shear stress, this fact is an indirect indication of a significant decrease in friction, which exhibits the same tendency as in the case of forced blowing.

It is more important that, by varying the velocity of the external pressure flow and the corresponding conditions at the inlet of the device, we can ensure the controlled air flow rate through the flow channel and perforated plate and, hence, blowing into the boundary layer. In this way, this passive air supply can be treated as a method for modifying the state and characteristic of the turbulent boundary layer on the surface past which it flows, which in turn makes it possible to estimate the efficiency of this control method for reducing friction.

Figure 5 shows the results of measurement of experimental values of the surface coefficient of friction in cross section $x = 1577$ mm in the form of the dependence $C_f = f(C_p)$, where $C_p = (P_{fp} - P_\infty)/q_\infty$ is the average (over the channel length) pressure coefficient. Here, the value of $C_p = 0$ corresponds to the conditions of damped inlet device. Clearly, the higher the pressure in the flow channel, the higher the rate of air flow through the wall and, hence, the lower the coefficient of friction C_f on the surface in the flow, which follows

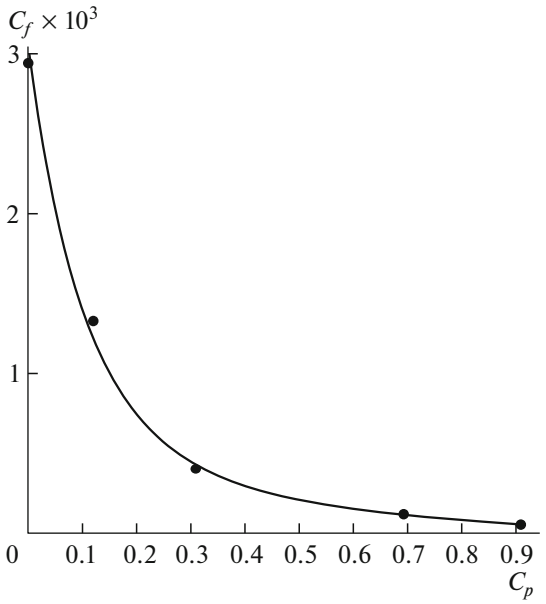

Fig. 5. Variation of the surface coefficient of friction in cross section $x = 1577$ mm ($\mathrm{Re}_x = 2.218 \times 10^6$) as a function of the averaged (over length) pressure coefficient in the flow channel.

from the above data. Interestingly, despite the significant reduction of friction at high values of C_p, the detached form of velocity profiles has not been obtained, but the predetached state of the boundary layer has already been attained.

Figure 6 shows analogous data that characterize the variations in surface coefficient of friction C_f upon the variations in the relative area of the discharge holes on the rear side of the flow channel. Here, the values of $F/F_{\mathrm{op}} = 0$ and 1 correspond to the completely close and open positions of the holes. It can be seen that, by changing the flow area of these holes, it is possible to vary C_f on the perforated surface over a wide range. This is clear because, e.g., upon an increase in ratio F/F_{op}, which is equivalent to a gradual increase in the flow area of the holes, a part of air is discharged into the external flow; the flow rate (and, hence the rate of blowing) of air through the permeable part of the plate into the boundary layer decrease accordingly. However, one should bear in mind that the throttling of the flow through circular holes can apparently cause considerable hydraulic losses that are comparable with the losses in the flow through a mesh arranged perpendicularly to the flow [19].

Figure 7 shows the results on the distribution of experimental values of surface coefficient of friction $C_f = f(x)$ along the plane plate with air flow (curve *1*) through the inlet device. The averaged data for the initial configuration (i.e., with damped inlet device) (*2*) are also shown for comparison. Results (*1*) were obtained for the averaged (over the area) blowing ratio

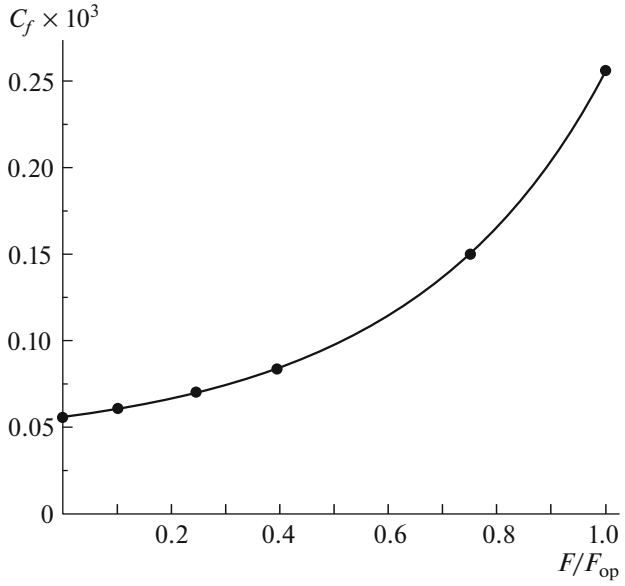

Fig. 6. Variation of the surface coefficient of friction in cross section $x = 1577$ mm ($Re_x = 2.218 \times 10^6$) as a function of the relative area of discharge holes.

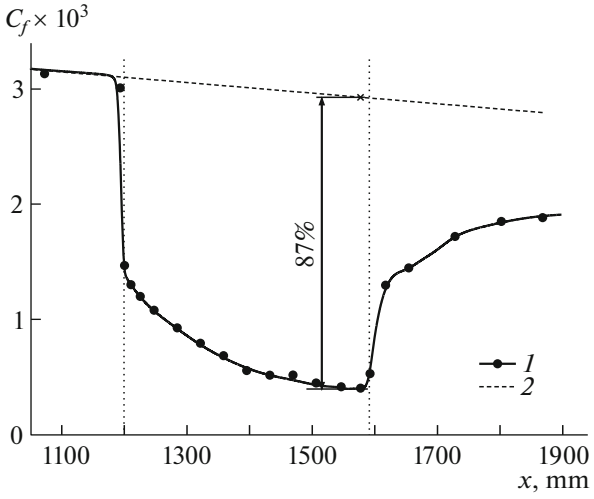

Fig. 7. Distribution of the surface coefficient of friction over the length of the model. $C_b = 3.95 \times 10^{-3}$ (*1*) and 0 (averaged experimental values) (*2*). Vertical dashed lines indicate the boundaries of the perforated sample.

$C_b = \rho_b v_b/\rho_\infty U_\infty = 3.95 \times 10^{-3}$. Since the value of C_b could not be measured directly, it was determined under the following assumption. In the course of previous experiments performed under the forced blowing of air into the boundary layer, we measured not only the air flow rate Q (by a precision flow meter), but also the pressure coefficient C_p in the pressure chamber; the relation between these quantities is shown in Fig. 8. Using this gauge dependence, we can easily determine flow rate Q (and, hence, the blowing ratio) from the measured values of C_p in the flow channel. Clearly, in these two cases, the peculiarities in the air supply do not allow us to treat them as completely identical. For this reason, the value of C_b obtained here generally requires refinement using independent methods.

It is noteworthy that the coefficient of surface friction decreases significantly, and this effect becomes stronger with increasing distance from the front face of the perforated sample (see Fig. 7). The strongest reduction of friction can be attained at the end of the perforated segment, in which the difference as compared to the initial flow (subscript "0") defined as $\Delta C_f/C_{f0} = (C_f - C_{f0})/C_{f0}$ amounts to about 80%. Analogous results (not given here) obtained at a higher density of the filter at the inlet to the flow channel indicate that the gain in friction becomes smaller.

With regard to the main mechanism of reducing friction, which was described in detail in [13], it becomes clear from an analysis of the profiles of integrated intensity of velocity pulsations $u'/v_* = f(y)$. It can briefly be described as follows. The pulsation profiles upstream from the perforated sample ($x = (1–2)\delta$ and higher) have basically the form typical of classical turbulent boundary layer, which appears as quite natural. On the perforated surface, the peak of velocity pulsations slightly increases in absolute value with increasing longitudinal coordinate x and is gradually displaced towards the outer side of the boundary layer. In this case, the distribution of u' over the boundary layer height is the same as detected before under forced blowing of air through the pressure chamber. This is characterized by the presence of at least two regions of the flow: with lower (compared to that in

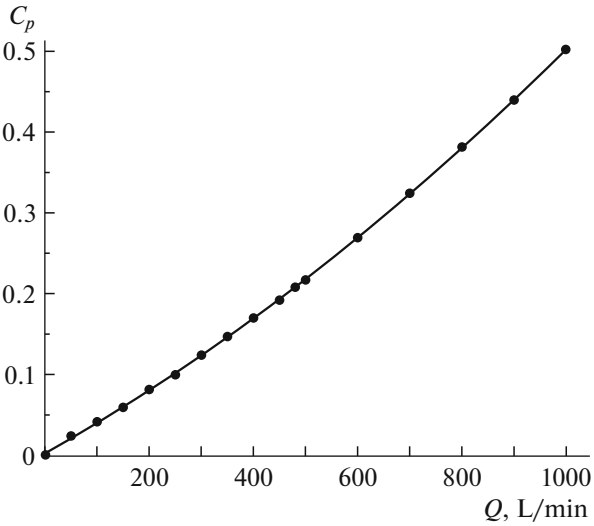

Fig. 8. Calibration data characterizing the dependence of the pressure coefficient in the pressure chamber on the air flow rate in the case of forced blowing.

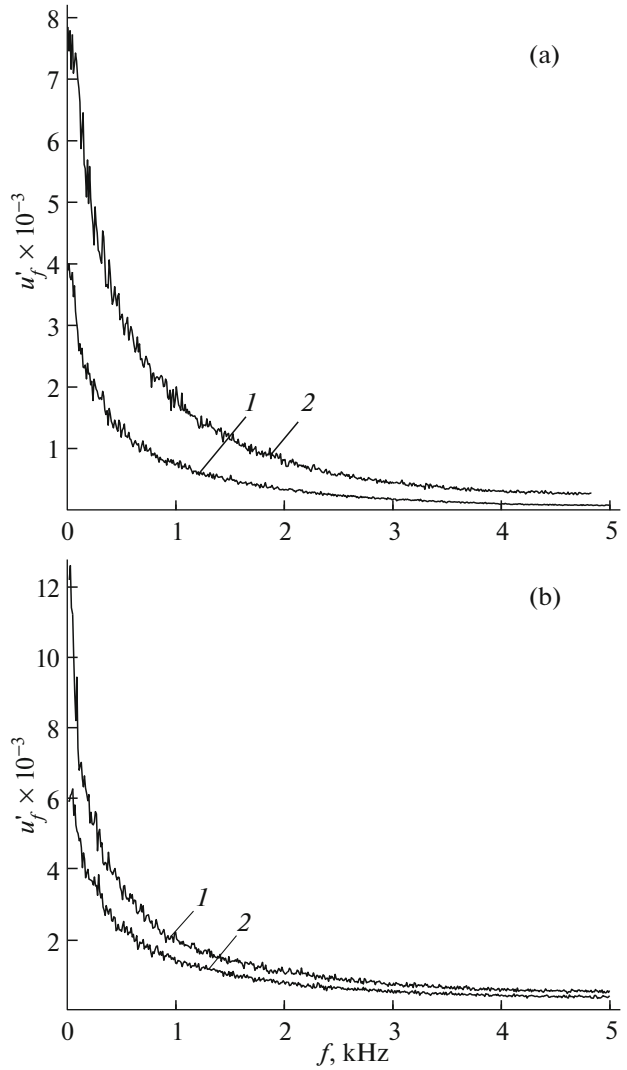

Fig. 9. Amplitude–frequency spectra of perturbations in the boundary layer in cross section $x = 1432$ mm ($\mathrm{Re}_x = 2.01 \times 10^6$) at distance (a) $y/\delta^{**} = 0.045$ from the wall and (b) $y/\delta^{**} = 2.20$. $C_b = 3.95 \times 10^{-3}$ (*1*) and 0 (*2*).

the initial flow) values of u' in the immediate vicinity of the wall and higher values of u' at larger distances from the wall. In the former case, this indicates that, in the presence of the flow through the inlet device, the maximum of turbulent velocity pulsations is shifted from the wall, which indicates an increase in the thickness of the viscous sublayer and, as a consequence, a decrease in surface friction.

This is confirmed by a comparison of the amplitude–frequency spectra of perturbations in the boundary layer shown in Fig. 9 in frequency band $\Delta f =$ 10 kHz in cross section $x = 1432$ mm for values $C_b = 0$ and $C_b = 3.95 \times 10^{-3}$ obtained at distance $y/\delta^{**} = 0.045$ from the wall (Fig. 9a), where the difference between the longitudinal velocity component pulsations for $C_b \neq 0$ and $C_b = 0$ is negative, and at distance

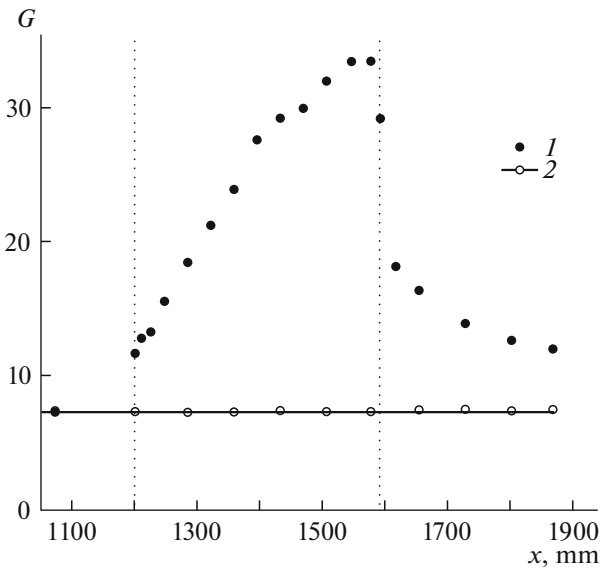

Fig. 10. Variation of the Causer equilibrium parameter over the length of the model. $C_b = 3.95 \times 10^{-3}$ (*1*) and 0 (*2*). Vertical dashed lines indicate the boundaries of the perforated sample.

$y/\delta^{**} = 2.20$ (Fig. 9b), where this difference is positive. It can be seen that, in the region of the flow located close to the wall (Fig. 9a), the level of perturbations in the entire frequency range is noticeably lower in the case of blowing, and the spectrum itself has the conventional form and, what is most important, has no preferred discrete frequencies. Conversely, upon an increase in relative coordinate y/δ^{**} (see Fig. 9b), the level of perturbations in the case of blowing is noticeably higher, but the spectrum does not contain preferred discrete frequencies either. It should be noted that a considerable change in the spectrum in the range of low frequencies, in which the perturbation intensity is substantially reduced (cf. distributions *1* and *2* in Fig. 9a) may indicate the degradation of low-frequency coherent structures due to passive blowing of air into the boundary layer.

As in all cases of forced blowing [7, 18], we observe the regions of lower values of C_f, embracing not only the perforated region proper, but also the impenetrable part of the plate located downstream. The form of the dependence $C_f = f(x)$ in this region is determined by two mechanisms:

(i) relaxation of the shear turbulent flow to its natural equilibrium (in the Clauser sense) state;

(ii) peculiarities of the flow at the permeable/impermeable wall boundary.

The former mechanism is confirmed by the form of the distribution of Clauser equilibrium parameter G over the model length (Fig. 10). It is well known that this parameter characterizes the balance between the turbulence kinetic energy generation and dissipation.

In the equilibrium state, this balance is observed, and quantity G has a constant value as in the case of the initial boundary layer (symbols *2*). However, another pattern of the flow is observed in the case of blowing (symbols *1*). It can be seen that the intersection of the front impermeable/permeable wall boundary, parameter G begins to increase from its equilibrium value, and this tendency is observed up to the permeable/impermeable wall boundary, after which it begins to decrease, approaching to its equilibrium (in the Clauser sense) value. Thus, the flow over the perforated surface and even downstream from it is in a strongly nonequilibrium state. As a rule, this type of flow is characterized by low values of friction [20].

The second mechanism can be described as follows. The natural increase in the thickness of the boundary layer in the direction of the x axis, which is enhanced due to air blowing, must obviously facilitate the rotation of the velocity vector above the perforated surface in the direction of the external flow. When the shear flow reaches the permeable/impermeable wall interface, the normal velocity component (at least, its part associated with the blowing) vanishes, which leads to the collapse of the flow with the formation of a vortex of the rolling type with angular velocity ω_z. This in turn slows down the increase in the surface friction in its tendency to the equilibrium state in a certain bounded region of the flow behind the perforated sample. Since energy sources for feeding the vortex no longer exist, its intensity decreases upon an increase in the longitudinal coordinate x, and ultimately dissipates completely. As a consequence, C_f gradually attains a corresponding value close to that in the equilibrium (in the Clauser sense) state.

It should be emphasized once again that the abovementioned wide region of the flow characterized by low values of friction behind the perforated sample is important for estimating the balance of the total aerodynamic drag of the plate/inlet device combination in the presence of air flow. Indeed, drag coefficient C_x of the model configuration under investigation can be represented in the most general case as the sum of the external drag coefficient C_{xw}, which is determined by the momentum loss in the boundary layer of the working surface, and the internal drag coefficient ΔC_x equivalent to the power spent for air blowing, the drag coefficient $C_{x\,\mathrm{inl}}$ of the inlet device itself, and the interference component $\Delta C_{x\,\mathrm{int}}$ of the plate/inlet device combination:

$$C_x = C_{xw} + \Delta C_x + C_{x\,\mathrm{inl}} + \Delta C_{x\,\mathrm{int}}.$$

The contributions of these components to the balance of the total aerodynamic drag are the subject of separate investigation. It should be noted, however, that since the first component is determined from the results of integration of dependence $C_f = f(x)$ along the plate, including the flow region behind the perforated sample also, we can obtain a significant additional gain in resistance. Component ΔC_x, which is equivalent to the additional power of the wind tunnel itself required for ensuring the passive air flow through the inlet device for a preset regime of the incoming flow, is apparently not large. The third component is determined to a considerable extent by the forces that act on the external surfaces of the inlet device, which depend on the nature of the flow past it, location, and type of fixation of the device on the plate, as well as the velocity of the flow and the quality of external enclosing of the device. In estimating the contribution of this component, it is difficult to avoid meticulous parametric calculations. In the general case, it is most difficult to determine the interference component of the plate/inlet device combination. This component is determined in most cases by separate measurements of forces and moments acting in the flow on aerodynamic elements subjected by interaction. Since in our case the inlet device is placed into the external flow, the value of this quantity is hopefully not very large.

CONCLUSIONS

1. The distribution of the main characteristics of the boundary layer under investigation (average velocity profiles, velocity pulsations, and the spectral composition of perturbations, integrated parameters of the flow, and local friction) in the case of the passive blowing of air through a fine-perforated wall using the resources of the external pressure flow is governed by the same regularities as in the case of forced blowing. This means that this form of air supply is a very reliable tool for acting on the turbulent boundary layer on the surface in the flow and for verifying its aerodynamic efficiency as a control method.

2. A stable decrease in the local values of the coefficient of surface friction C_f was observed over the length of the model, which can attain about 80% at the end of the perforated region for $C_b = 3.95 \times 10^{-3}$. A possibility of the further reduction of C_f by perfecting this method for controlling the boundary layer is preserved.

3. The proposed configuration of the flow channel of the inlet device can ensure an admissible air-flow rate through the perforated wall only in a relatively narrow range of flow velocities, which is quite natural. Parametric analysis should be performed by numerical methods that provide preliminary information on the optimal configuration of the flow channel in a wide range of the experimental conditions, which can be used directly in the experiment more effective control over the boundary layer.

Thus, our results indicate that in the method of controlling the turbulent boundary layer considered here, the forced air supply is not a must. The controllable air flow rate through the flow channel, permeable wall, and further to the boundary layer required to control the distribution and magnitude of the surface

friction on the surface in the flow can be ensured by varying the velocity of the external pressure flow and the conditions at the inlet of the feeding device. This approach is a simple and accessible tool for solving the posed problem, which makes it theoretically possible to reduce the weight of the entire structure as compared to that in the case of forced air feed.

ACKNOWLEDGMENTS

This work was supported in part by the Russian Foundation for Basic Research (project no. 14-08-00020).

REFERENCES

1. R. Wood, SAE Int. TP-2004-01-1306 (2004).
2. A. Abbas, J. de Vicente, and E. Valero, Aerosp. Sci. Technol. **28**, 100 (2013).
3. W. K. Lord, S. H. Zysman, T. G. Tillman, and W. A. Johnson, *Laminar flow control experiment on a large-scale nacelle model*, Pratt & Whitney Rep. PWA 6420-55 (December 1995).
4. D. M. Bushnell, Proc. Inst. Mech. Eng., IMechE Conf. **G00602**, 1 (2003).
5. D. Hwang, Progr. Aerosp. Sci. **40**, 559 (2004).
6. T. G. Tillman and D. P. Hwang, in *Proceedings of the 37th AIAA Aerospace Sciences Meeting and Exhibit, Reno, 1999,* AIAA Pap. No. 1999-0130.
7. V. I. Kornilov and A. V. Boiko, AIAA J. **50**, 724 (2012).
8. Y. L. Lin, M. K. Chyu, T. I. P. Shih, B. P. Willis, and D. P. Hwang, AIAA Pap. No. 98-0359.
9. J. Li, C.-H. Lee, L. Jia, and X. Li, in *Proceedings of the 47th AIAA Aerospace Sciences Meeting, Orlando, 2009,* AIAA Pap. No. 2009-779.
10. V. I. Kornilov, Progr. Aerosp. Sci. **76**, 1 (2015).
11. F. A. P. Silva, D. O. A. Cruz, and C. C. Pellegini, Int. J. Heat Mass Transf. **38**(13), 2507 (1995).
12. J. Bellettre, F. Bataille, and A. Lallemand, Int. J. Therm. Sci. **38**, 492 (1999).
13. V. I. Kornilov, A. V. Boiko, and I. N. Kavun, Inzh.-Fiz. Zh. **88**, 1448 (2015).
14. D. Hwang, in *Proceedings of the 23rd Congress of the International Council of the Aeronautical Sciences, Toronto, 2002,* Ed. by I. Grant (Optimage, 2002), pp. 2101.1–2101.7.
15. A. V. Boiko and V. I. Kornilov, Teplofiz. Aeromekh. **17**, 613 (2010).
16. T. Cebeci, *Analysis of Turbulent Flows* (Elsevier, Oxford, 2004).
17. *Proceedings of the Stanford Conference AFOSR-IFP, Stanford,* 1969, Ed. by D. E. Coles and E. A. Hirst (Stanford Univ., Stanford, 1969), Vol. 2.
18. V. I. Kornilov and A. V. Boiko, AIAA J. **52** (1), 93 (2014).
19. I. E. Idel'chik, *A Handbook of Hydraulic Resistance* (Mashinostroenie, Moscow, 1975).
20. V. I. Kornilov and D. K. Mekler, Izv. Sib. Otd. Akad. Nauk SSSR, Ser. Tekh. Nauk, No. 6, 38 (1989).

Translated by N. Wadhwa